

1

Supporting Information

2 **Ostwald ripening mechanism-derived MnOOH induces lattice** 3 **oxygen escape for efficient aqueous MnO₂-Zn batteries**

4 Junjie Zheng,^{a,c} Chenchen Qin,^c Chi Chen,^{a,*} Chuankun Zhang,^d Pei Shi,^{a,c} Xin Chen,^c Yi Gan,^c

5 Jingying Li,^c Jia Yao,^c Xin Liu,^c Junyan Cheng,^c Dan Sun,^a Houzhaow Wan^{b,c,*}, Hao Wang^{b,c,*}

6 ^a CAS Key Laboratory of Design and Assembly of Functional Nanostructures, and Fujian

7 Provincial Key Laboratory of Nanomaterials, Fujian Institute of Research on the Structure of

8 Matter, Chinese Academy of Sciences, Fuzhou 350002, China.

9 ^b Hubei Yangtze Memory Laboratories, Wuhan 430205, China.

10 ^c Hubei Key Laboratory of Micro-Nanoelectronic Materials and Devices, School of

11 Microelectronics, Hubei University, Wuhan, 430062, PR China.

12 ^d Hubei Key Laboratory of Energy Storage and Power Battery, School of Mathematics, Physics

13 and Optoelectronic Engineering, Hubei University of Automotive Technology, Shiyan 442002,

14 PR China.

15 * Corresponding authors, E-mail: xmchenchi@fjirsm.ac.cn (C. Chen); houzhaow@hubu.edu.cn

16 (H. Wan); nanoguy@126.com, wangh@hubu.edu.cn (H. Wang)

17

18 **Experimental methods**

19 *Chemicals:* Mineral chameleon (KMnO₄), Polyethylene glycol 400 (HO(CH₂CH₂O)_nH), Zinc

20 vitriol (ZnSO₄·7H₂O), Mn hydrate sulfate (MnSO₄·H₂O), Zinc plate, All raw materials purchased

21 are of analytical grade and have not been purified before use.

22

23 *Preparation of the MnOOH nanorods:* Weigh 0.15 g of potassium permanganate (KMnO₄) with

1 weighing paper at room temperature and put it into a cleaned beaker, weigh 60 ml of deionized
2 water in a graduated cylinder and pour it into the beaker. Use a pipette gun to take 3 ml of
3 polyethylene glycol (PEG-400) and drop it into the solution, stir for 30 minutes, then put the
4 completely dissolved solution in a dry box to react at 160°C for 5 h. After the reaction was
5 completed, rinse with deionized water and ethanol, and collect the filtered powder sample with
6 filter paper to obtain manganese oxyhydroxide (MnOOH) nanorods.

7

8 *Preparation of the MnO₂ (O_d) nanorods:* The prepared precursor MnOOH was placed in a high-
9 temperature sintering furnace to react in an air atmosphere at different temperatures. The
10 temperature was raised at 2 °C/min, and the temperature was raised to a constant temperature of
11 280°C, 300°C, 350°C, 400°C, 450°C, and 550°C, respectively, and the heat treatment time was set
12 to 2 h. After the reaction is completed, the powder samples are collected separately to obtain
13 manganese dioxide (MnO₂) nanorods.

14

15 *Structural characterization:* X-ray diffraction (XRD) is a diffractometer obtained by
16 Bruker D8 Advance using 40 kV, 40 mA CuK α radiation. A scanning electron microscope (SEM,
17 JEOL JSM-7100F) was used to study the morphology and size of the samples. Using a cold field
18 emission electron source and an image Cs corrector (CEOS GmbH), A JEOL ARM 200 F
19 microscope operating at 200 kV was tested on a transmission electron microscope (TEM) and
20 energy dispersive X-ray spectrometer (EDX). X-ray photoelectron spectrometer (XPS) was
21 performed using a Thermo Fisher Scientific Escalab 250Xi spectrometer with AlK α radiation.

22

1 Computational details

2 Our first-principle calculations are performed using VASP code[1], based on density-
3 functional theory (DFT)[2, 3]. The $2 \times 2 \times 3$ supercells of β -MnO₂ are chosen as calculation
4 models. The exchange–correlation energy is calculated using general gradient approximation
5 (GGA) with the Perdue–Burke–Ernzerhof (PBE) exchange–correlation functional[4]. The DFT+U
6 method[5, 6] including strong correlation effects was adopted to describe the localized Mn-3d
7 electrons and the U-J values are set to 3.9 eV[7]. The effect of van der Waals interactions was
8 estimated, implemented in the optimized exchange van der Waals functional DFT-D3[8]. The
9 plane wave cutoff energy is 520 eV and the k-point meshes of $3 \times 3 \times 3$ and $5 \times 5 \times 5$ in the
10 Monkhorst Pack[9] sampling scheme are used for geometry optimization and computation of
11 electronic properties, respectively. The convergence condition for the energy is 10^{-5} eV, and the
12 structures were relaxed until the force on each atom is less than 0.01 eV/Å. Spin polarization is
13 considered in all calculations. And the structure drawing and charge density visualization were
14 generated using VESTA[10].

15 The binding energies E_b of H are defined as:

$$16 \quad E_b = E(\text{MnO}_2 + \text{H}) - (E(\text{MnO}_2) + E(\text{H})),$$

17 here, $E(\text{MnO}_2 + \text{H})$ is the total energy of pristine or defective MnO₂ with a H adatom,
18 $E(\text{MnO}_2)$ is the total energy of pristine or defective MnO₂ and $E(\text{H}) = 1/2 E(\text{H}_2)$; $E(\text{H}_2)$ is the total
19 energy of the total energy of H₂ molecule.

20

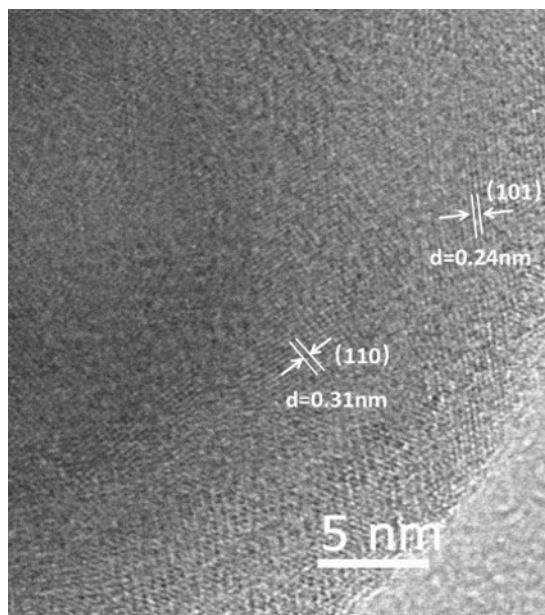
1 **Results and Discussion**

2



3 **Figure S1.** Preparation schematic of β - MnO_2 (O_d) electrode material.

4



5

6 **Figure S2.** HR-TEM image of β - MnO_2 (O_d).

7

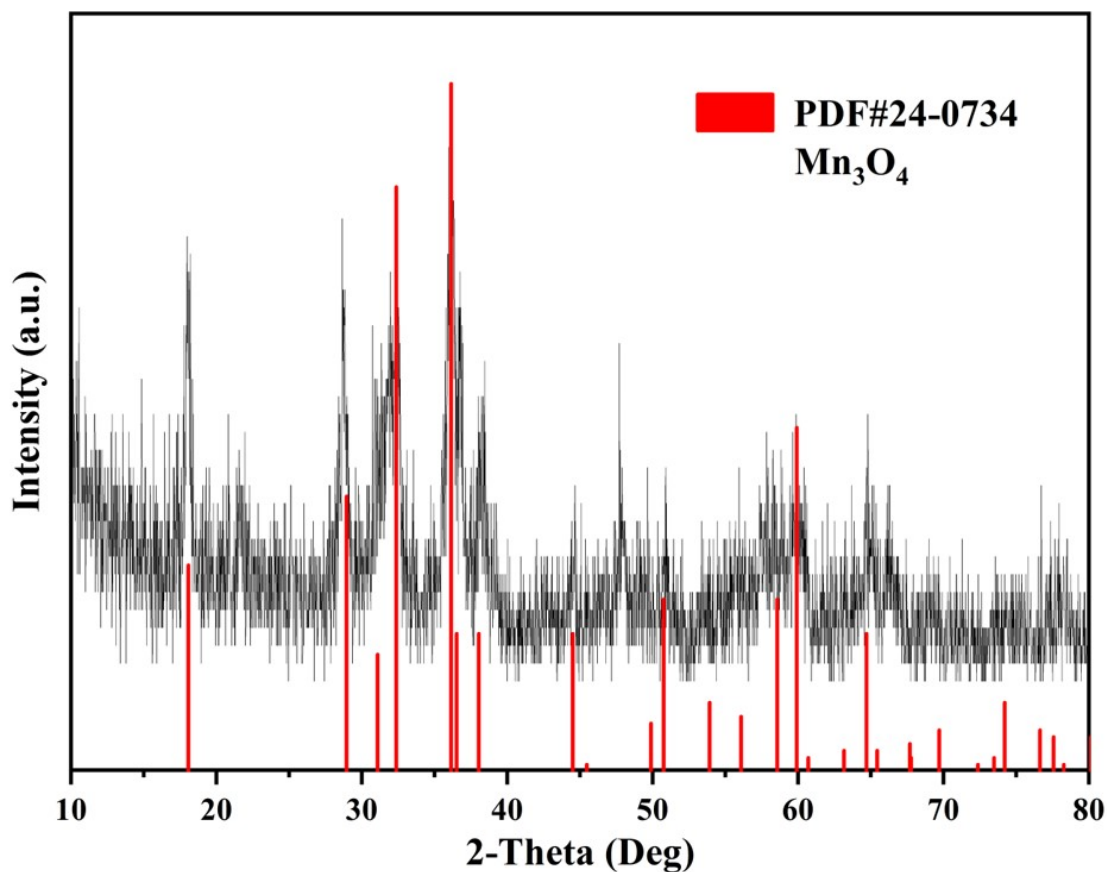
Element	Line type	wt%	wt% sigma	Atomic percentage
O	K type	40.52	0.40	64.33
Mn	K type	54.54	0.40	25.22
C	K type	4.94	0.26	10.45
Total		100.00		100.00

8

1 **Figure S3.** Elemental content of β - MnO_2 (O_d).

2

3

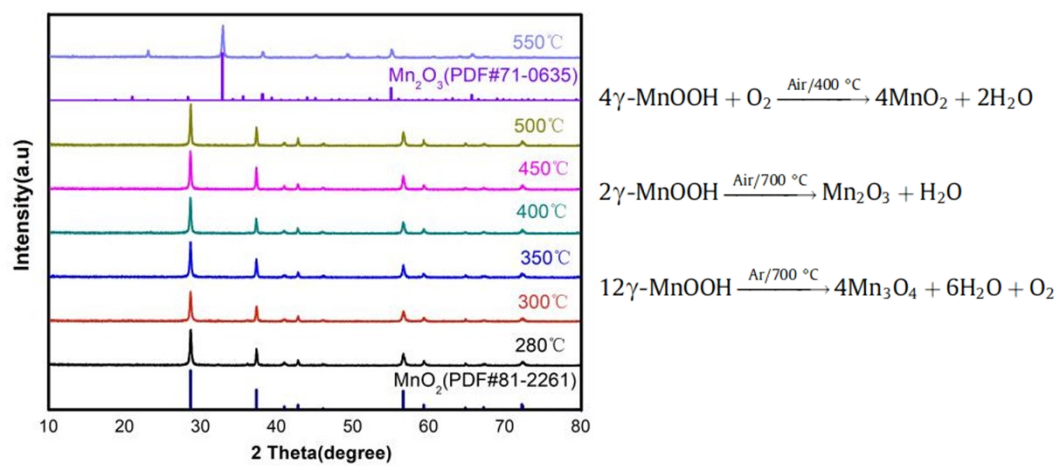


4

5 **Figure S4.** XRD pattern of Mn_3O_4 after heat treatment in inert gas.

6

7

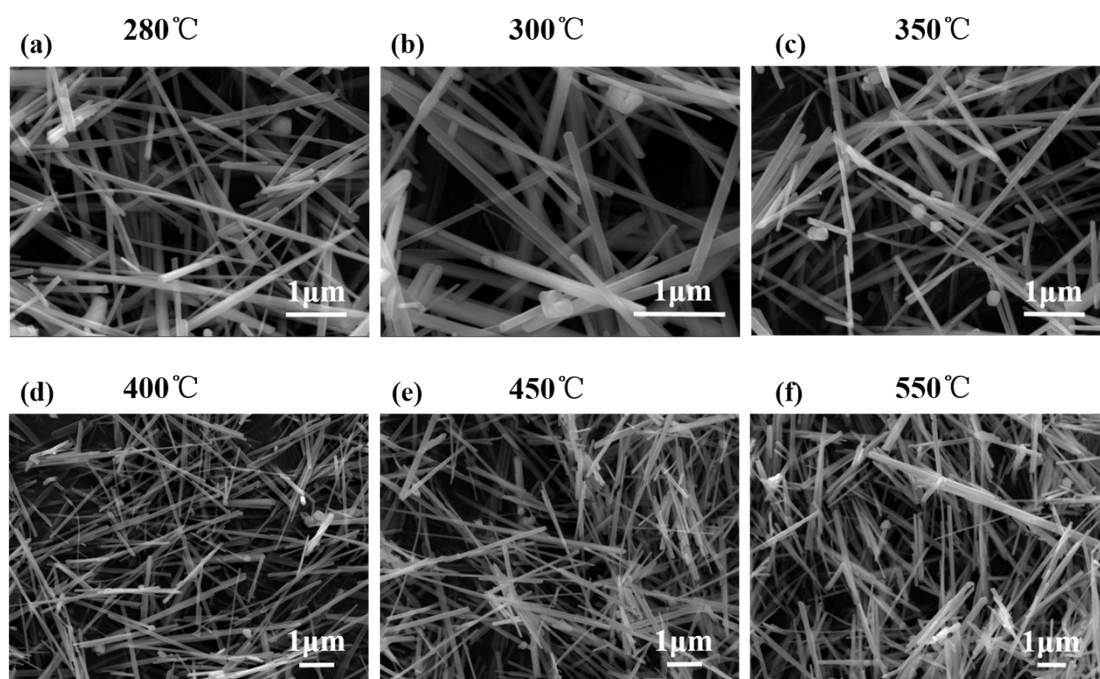


8

1 **Figure S5.** XRD patterns of MnOOH after heat treatment at different temperatures in air.

2

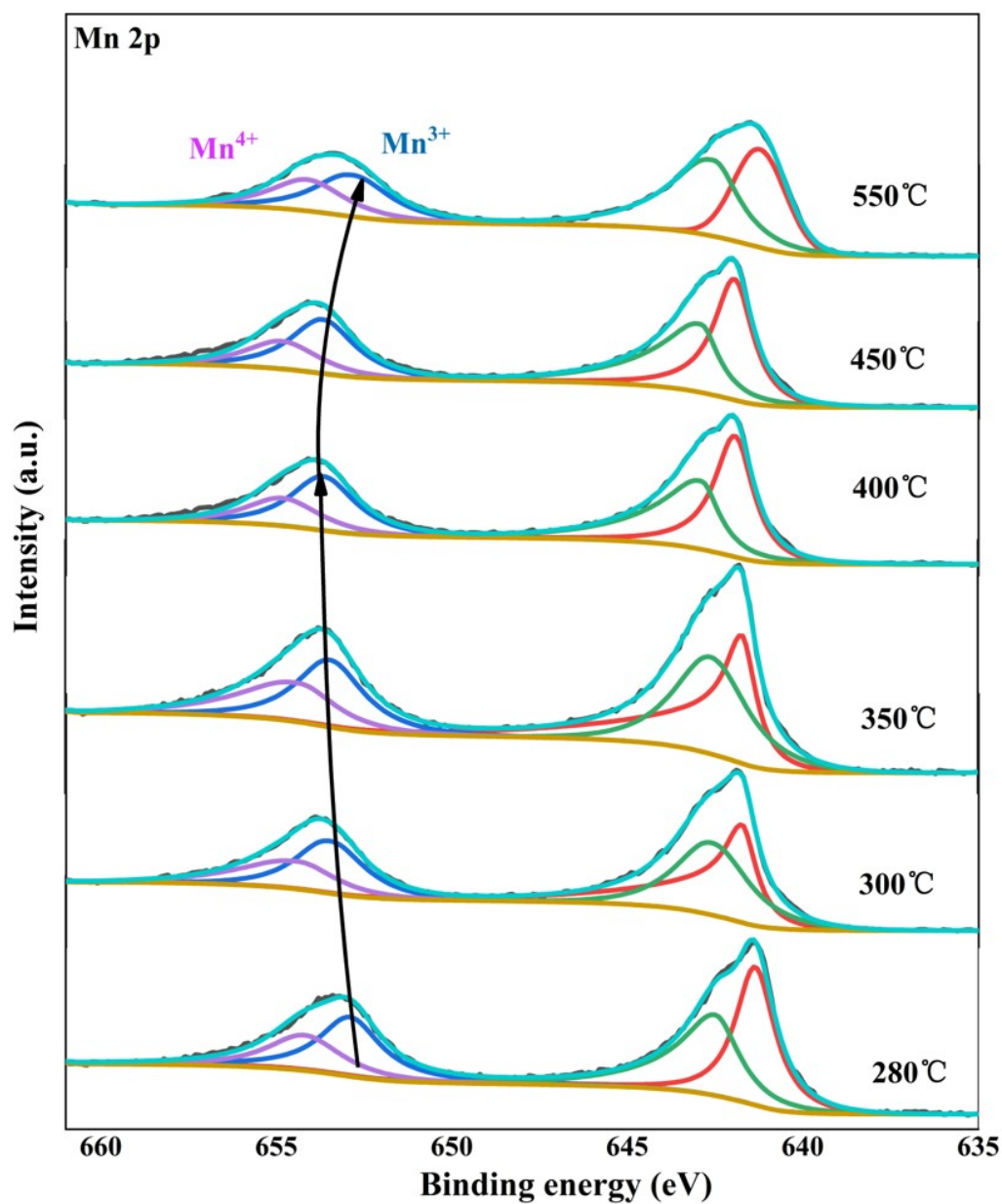
3



5 **Figure S6.** SEM images of MnOOH after heat treatment at different temperatures in air.

6

7



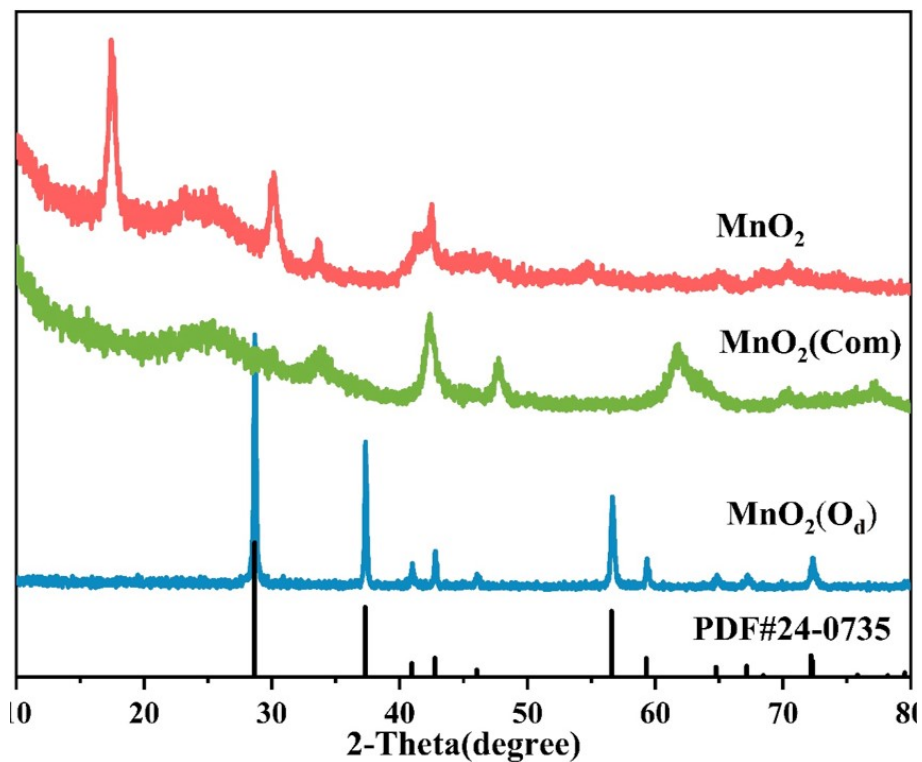
1

2 **Figure S7.** XPS changes of Mn elements in the products of MnOOH after heat treatment at

3 different temperatures in air.

4

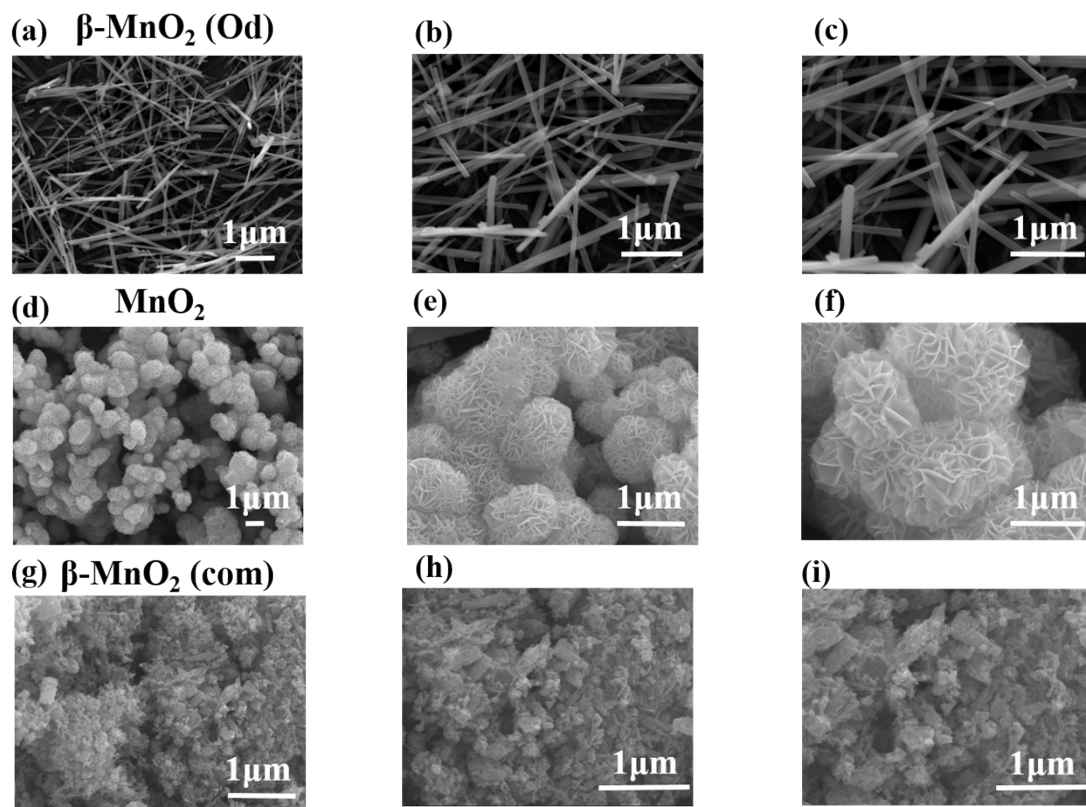
5



1

2 **Figure S8.** XRD comparison chart of β - MnO_2 (O_d), MnO_2 (com), MnO_2 three materials.

3



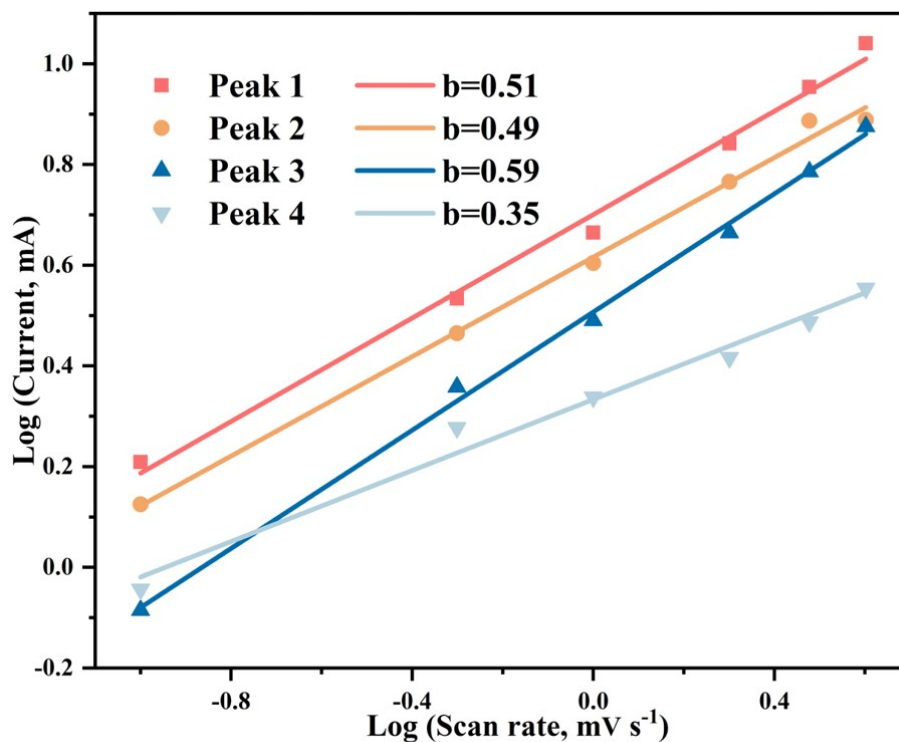
4

5 **Figure S9.** SEM comparison chart of β - MnO_2 (O_d), MnO_2 (com), MnO_2 three materials.

1 For further explore energy storage mechanism of the β -MnO₂ (O_d) in different electrolyte, the
2 formula for analyzing CV data at various scan rates according to a typical method[11] is as
3 follows:

$$4 \quad i = av^b$$

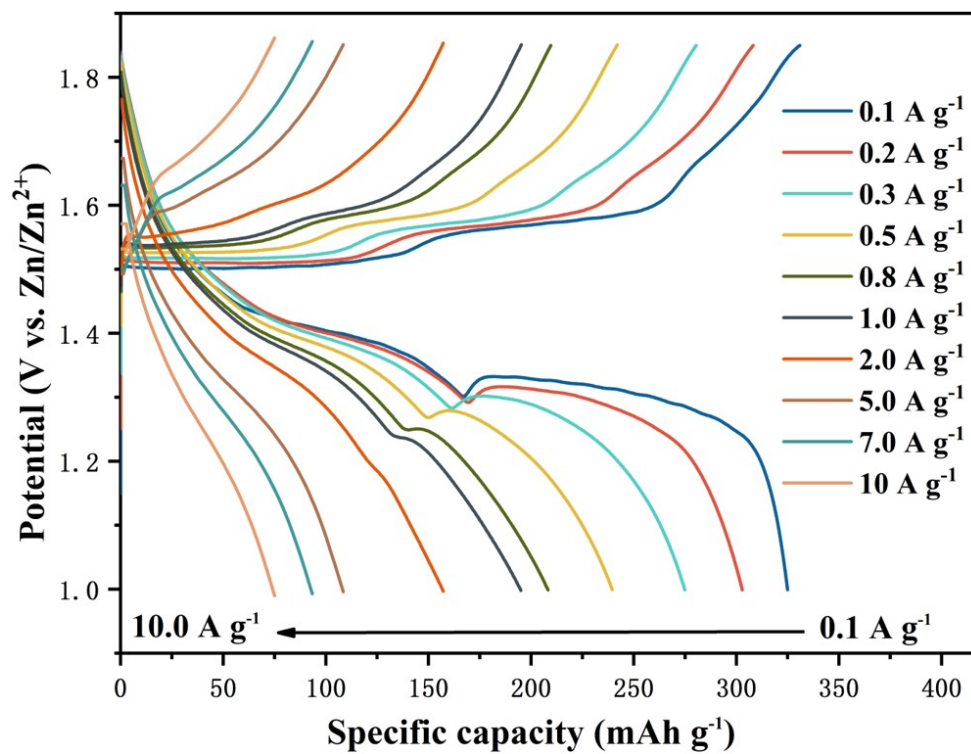
5 The measured current (*i*) corresponds to the power-law relationship of the scan rate (*v*). *a* and *b*
6 are tunable parameters, where *b* is a value determined by the slope of the relationship between $\log i$
7 and $\log v$, the coefficient *b* varies in the range of 0.5-1.0, so there are two clearly defined
8 conditions, namely *b* = 0.5 and *b* = 1.0. The *b* value is 0.5, which indicates the insertion process of
9 diffusion control, and the *b* value is 1.0, which indicates the surface capacitance process. Linear
10 relationship between $\log i$ and $\log v$ graphs ($\log i = \log a + b \log v$) according to **Figure S10**[12].
11 The *b* values of the four redox peaks are calculated to be 0.51 (peak 1), 0.49 (peak 2), 0.59 (peak 3)
12 and 0.35 (peak 4), This indicates that the electrochemical kinetics of the compounds are related to
13 diffusion-controlled processes and capacitive effects, but capacitive effects are the main process.



1

2 **Figure S10.** *b*-value of β -MnO₂ (O_d) fitted by CV curve.

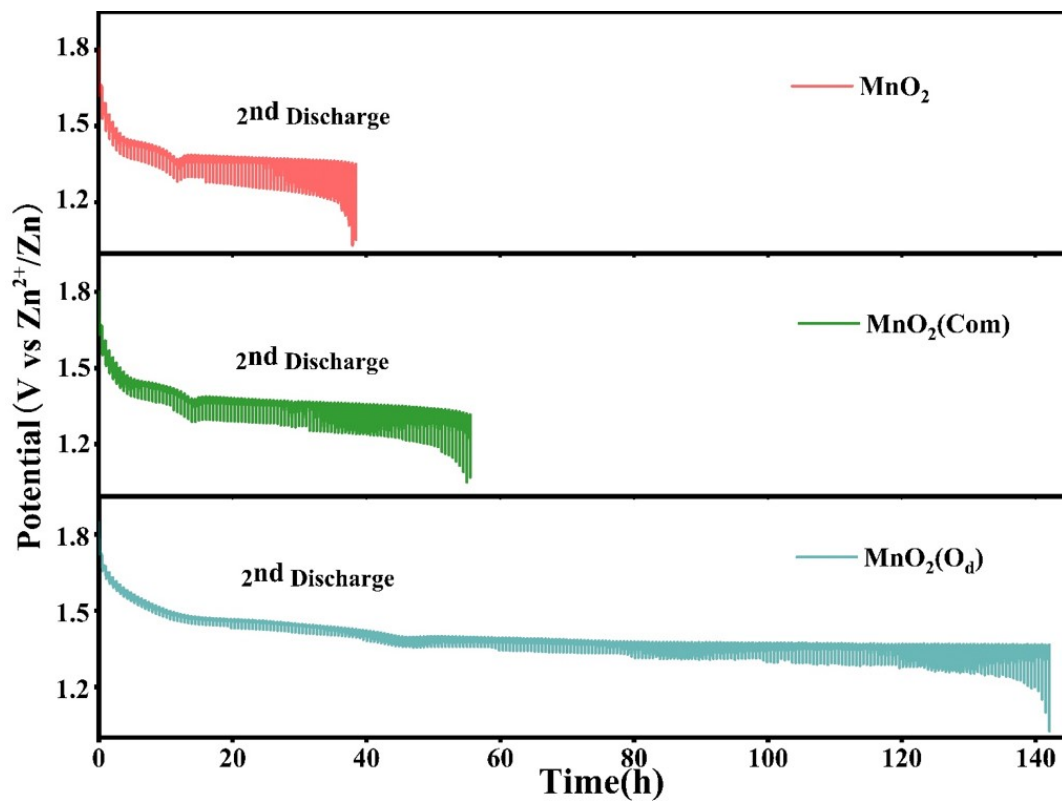
3



4

5 **Figure S11.** GCD curve of Zn// β -MnO₂ (O_d) battery.

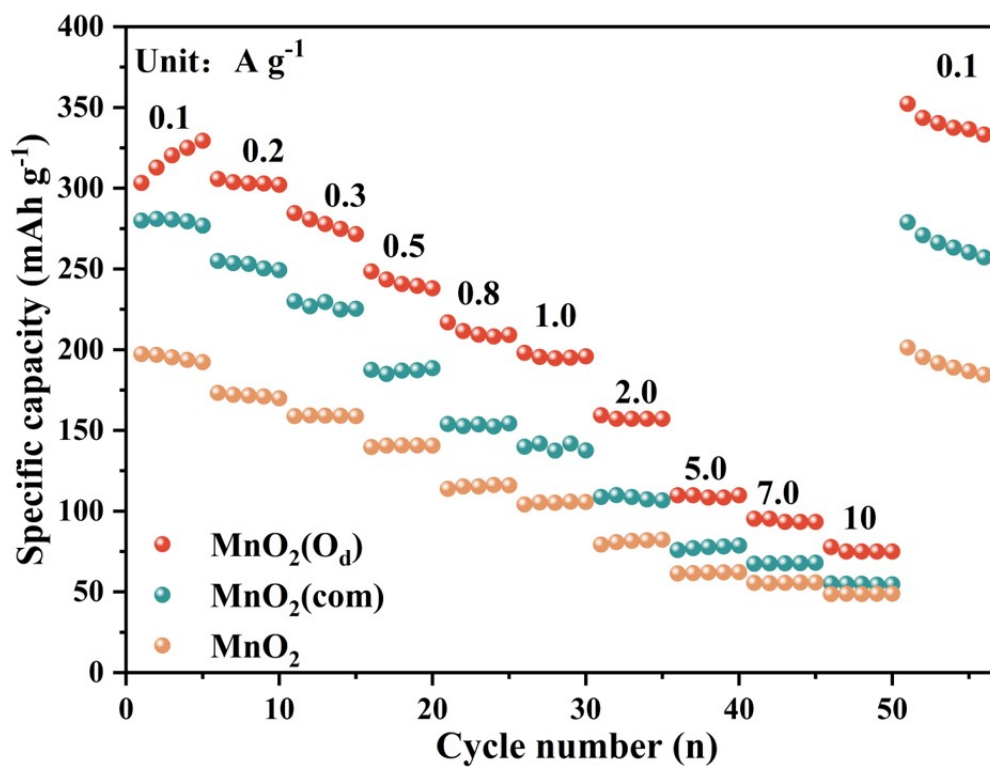
6



1

2 **Figure S12.** GITT comparison chart of three different materials.

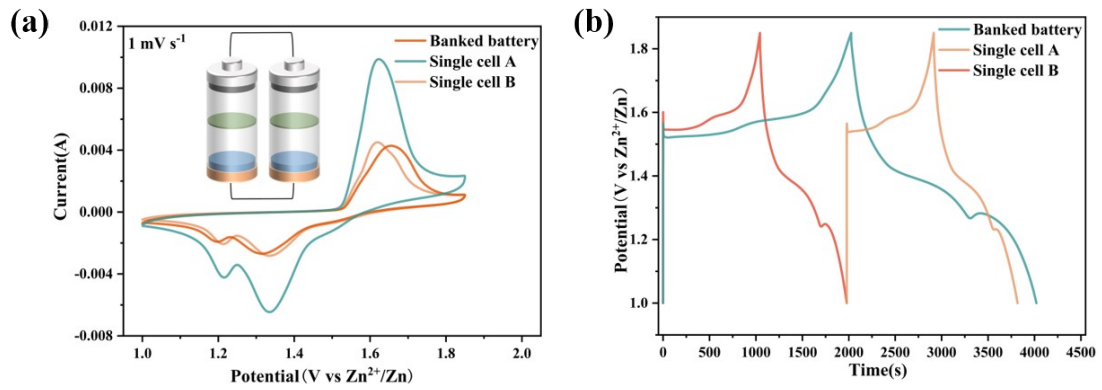
3



4

5 **Figure S13.** Comparison chart of rate performance of three different materials.

1



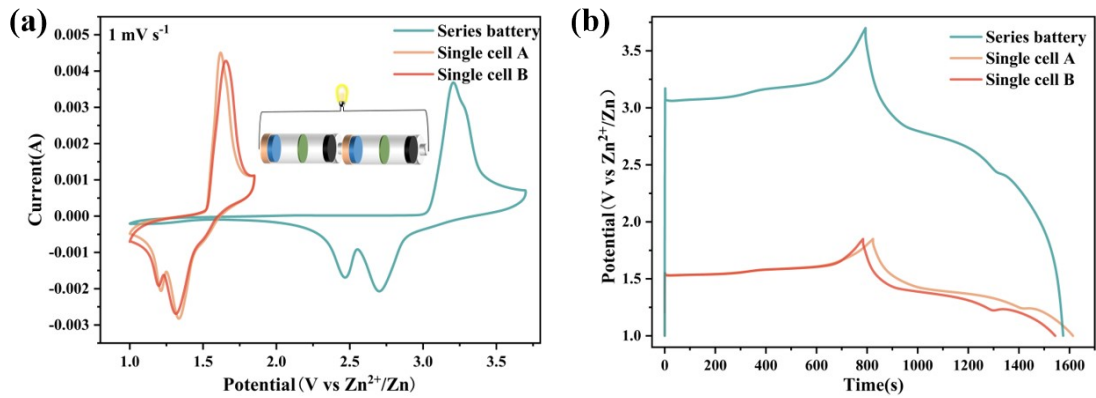
2

3 **Figure S14.** a) CV curves of Zn//β-MnO₂ (O_d) single pouch battery and parallel connection. b)

4 GCD curves of Zn//β-MnO₂ (O_d) single pouch battery and parallel connection.

5

6



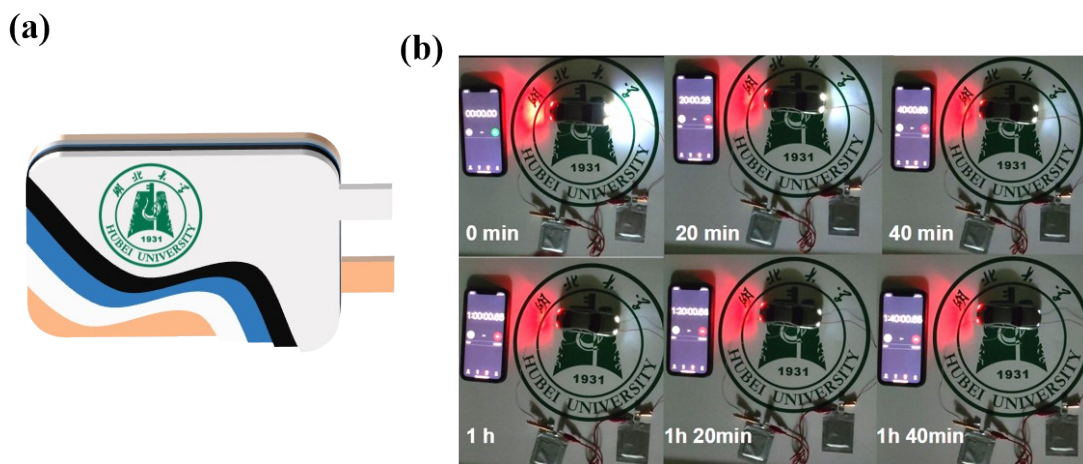
7

8 **Figure S15.** a) CV curves of Zn//β-MnO₂ (O_d) single pouch battery and series connection. b)

9 GCD curves of Zn//β-MnO₂ (O_d) single pouch battery and series connection.

10

11



1

2 **Figure S16.** a) Schematic diagram of pouch battery. b) Zn//β-MnO₂ (O_d) soft pack batteries are

3 connected in series to light up the car model lights.

4 **References**

5 [1] G. Kresse, J. Furthmüller, J. Hafner, Theory of the crystal structures of selenium and tellurium: The
 6 effect of generalized-gradient corrections to the local-density approximation, *Physical Review B*, 50(18)
 7 (1994), 13181-13185. <https://doi.org/10.1103/PhysRevB.50.13181>.

8 [2] P. Hohenberg, W. Kohn, Inhomogeneous Electron Gas, *Physical Review*, 136(3B) (1964), B864-
 9 B871. <https://doi.org/10.1103/PhysRev.136.B864>.

10 [3] L.J. Sham, W. Kohn, One-Particle Properties of an Inhomogeneous Interacting Electron Gas,
 11 *Physical Review*, 145(2) (1966), 561-567. <https://doi.org/10.1103/PhysRev.145.561>.

12 [4] J.P. Perdew, K. Burke, M. Ernzerhof, Generalized Gradient Approximation Made Simple *Phys. Rev.*
 13 *Lett.* 77, 3865 (1996), *Physical Review Letters*, 78(7) (1997), 1396-1396.
 14 <https://doi.org/10.1103/PhysRevLett.78.1396>.

15 [5] S.L. Dudarev, A.I. Liechtenstein, M.R. Castell, G.A.D. Briggs, A.P. Sutton, Surface states on NiO
 16 (100) and the origin of the contrast reversal in atomically resolved scanning tunneling microscope
 17 images, *Physical Review B*, 56(8) (1997), 4900-4908. <https://doi.org/10.1103/PhysRevB.56.4900>.

- 1 [6] A.I. Liechtenstein, V.I. Anisimov, J. Zaanen, Density-functional theory and strong interactions:
2 Orbital ordering in Mott-Hubbard insulators, *Physical Review B*, 52(8) (1995), R5467-R5470.
3 <https://doi.org/10.1103/PhysRevB.52.R5467>.
- 4 [7] A. Jain, G. Hautier, C.J. Moore, S. Ping Ong, C.C. Fischer, T. Mueller, K.A. Persson, G. Ceder, A
5 high-throughput infrastructure for density functional theory calculations, *Computational Materials*
6 *Science*, 50(8) (2011), 2295-2310. [https://doi.org/https://doi.org/10.1016/j.commatsci.2011.02.023](https://doi.org/10.1016/j.commatsci.2011.02.023).
- 7 [8] S. Grimme, J. Antony, S. Ehrlich, H. Krieg, A consistent and accurate ab initio parametrization of
8 density functional dispersion correction (DFT-D) for the 94 elements H-Pu, *The Journal of Chemical*
9 *Physics*, 132(15) (2010), 154104. <https://doi.org/10.1063/1.3382344>.
- 10 [9] H.J. Monkhorst, J.D. Pack, Special points for Brillouin-zone integrations, *Physical Review B*, 13(12)
11 (1976), 5188-5192. <https://doi.org/10.1103/PhysRevB.13.5188>.
- 12 [10] K. Momma, F. Izumi, VESTA: a three-dimensional visualization system for electronic and
13 structural analysis, *Journal of Applied Crystallography*, 41(3) (2008), 653-658.
14 [https://doi.org/https://doi.org/10.1107/S0021889808012016](https://doi.org/10.1107/S0021889808012016).
- 15 [11] V. Augustyn, J. Come, M.A. Lowe, J.W. Kim, P.-L. Taberna, S.H. Tolbert, H.D. Abruña, P.
16 Simon, B. Dunn, High-rate electrochemical energy storage through Li⁺ intercalation pseudocapacitance,
17 *Nature Materials*, 12(6) (2013), 518-522. <https://doi.org/10.1038/nmat3601>.
- 18 [12] T. Brezesinski, J. Wang, J. Polleux, B. Dunn, S.H. Tolbert, Templated Nanocrystal-Based Porous
19 TiO₂ Films for Next-Generation Electrochemical Capacitors, *Journal of the American Chemical*
20 *Society*, 131(5) (2009), 1802-1809. <https://doi.org/10.1021/ja8057309>.

21

22